2022

Effects of Shell Hash on Friction Angles of Surficial Seafloor Sediments near Oysters

Samuel T. Consolvo

Nina Stark

(...)

Grace M. Massey
Virginia Institute of Marine Science

Recommended Citation

Consolvo, Samuel T.; Stark, Nina; (...); and Massey, Grace M., Effects of Shell Hash on Friction Angles of Surficial Seafloor Sediments near Oysters (2022). *Journal of Waterway, Port, Coastal, and Ocean Engineering*, 148(5), 04022015.
doi: 10.1061/(ASCE)WW.1943-5460.0000716.

Effects of Shell Hash on Friction Angles of Surficial Seafloor Sediments near Oysters

Samuel T. Consolvo, A.M.ASCE[1]; Nina Stark, Ph.D., M.ASCE[2]; Bernardo Castellanos, Ph.D., M.ASCE[3]; Celso F. Castro-Bolinaga, Ph.D., A.M.ASCE[4]; Steven Hall, Ph.D., P.E., M.ASCE[5]; and Grace Massey, Ph.D.[6]

Abstract: Oysters are hypothesized to affect the shear strength of nearby surficial seafloor sediment as fragments of oyster shells (shell hash) are typically more angular relative to sand particles alone, among other differences. Resistance to shearing is well characterized by the friction angle, which is estimated in this study from vacuum triaxial laboratory and portable free-fall penetrometer field tests. Friction angles of sediment with shell hash were higher relative to those of sediment without shell hash (via hydrochloric acid treatment) on average by about 19% (36.0°–30.2°, respectively). Triaxial confining pressures ranged between 2.1 and 49.0 kPa to simulate subtidal and intertidal aquatic conditions. Regularity (average of particle roundness and sphericity) values of sediment samples with shell hash were found to be less than those of samples without by about 6% (0.66 and 0.70, respectively), which indicates the particle shapes of the former are, overall, more angular and less spherical. Further study and methodology improvements are needed to decrease the approximate 9° friction angle discrepancy estimated from field- and laboratory-based tests. Knowing oysters have the potential to increase sediment shearing resistance helps establish a pathway of how shellfish colonies may contribute to mitigating surficial erosion around coastal infrastructure.
DOI: 10.1061/(ASCE)WW.1943-5460.0000716.

Introduction

The potential increase of sediment shear strength associated with the presence of bivalve (e.g., oyster, mussel, and scallop) shells is investigated here, evaluating a pathway of how shellfish colonies may contribute to mitigating surficial erosion in aquatic environments in addition to decreasing flow from surface roughness, among other functions. The need to protect infrastructure from erosion and scour has been well documented and is critical to long-term serviceability (Chiew 1992; Briaud et al. 1999; Pagán-Ortiz 2002; Arneson et al. 2012). Traditional erosion protection measures, such as placement of riprap stones, installation of a collar around a pier, and the use of pier slots, have many challenges. These include difficulties replicating riprap field conditions with small-scale laboratory experiments (Johnson and Ayyub 1996), significant fluctuations in bed surface elevation that could compromise the effectiveness of a pier collar (Chiew 1992), and flow direction mischaracterizations that could make a pier slot ineffective (Kumar et al. 1999). Negative environmental and ecological impacts from riprap placement must not be overlooked either. Reid and Church (2015) noted that increased channel bed scouring, downstream erosion, and detrimental effects on vertebrate habitats are more likely to occur from large quantities of riprap placement. These challenges with traditional erosion protection measures can be potentially alleviated by the implementation of bioengineered, self-sustaining contiguous mats of interconnected bivalve colonies that attract larval settlement in scour-prone areas. Although the implementation of this biologically engineered solution is not the focus of this paper, it is important to highlight for the purposes of explaining the motivation behind this study. Furthermore, use of bivalves does not have to be limited to scour mitigation, but can possibly help with benthic life habitat, slope stabilization, and beach erosion (Meyer et al. 1997; Coen et al. 2007; Abel et al. 2019).

Bivalve colonies have been shown to withstand water velocities on the order of 6 m/s with less than a 10% probability of dislodgement (Hunt and Scheibling 2001). For context, a boulder with its longest dimension of approximately 5 m requires a minimum flow velocity on the order of 10 m/s to initiate transport (Nandasena et al. 2011), or about 1.5 m/s is required to scour the bed and banks of a shallow (<1 m) open channel comprised of cobble- and shingle-sized substrate (Fortier and Scobey 1926). As a geotechnical insight into the viability of using oyster reefs as a bioengineered scour solution, this paper focuses on the degree to which the varying amounts of oyster shell fragments effect sediments' ability to resist shear stresses in terms of the friction angle estimated from laboratory and field testing. It should be noted that shell fragments are not exclusively found near bivalve colonies (Kwag et al. 1999); however, an abundance of broken shell material intermixed with the in situ surficial sediment can be expected near a bivalve colony.

Even small weight fractions of angular particles intermixed with rounded sand particles can have a significant influence

[1]Geotechnical Engineer, CDM Smith Inc., Boston, MA 02109; previously at Dept. of Civil and Environmental Engineering, Virginia Tech, Blacksburg, VA 24061 (corresponding author). Email: samueltc@vt.edu

[2]Associate Professor, Dept. of Civil and Environmental Engineering, Virginia Tech, Blacksburg, VA 24061. ORCID: https://orcid.org/0000-0001-9484-069X

[3]Research Scientist, Dept. of Civil and Environmental Engineering, Virginia Tech, Blacksburg, VA 24061.

[4]Assistant Professor, Dept. of Biological and Agricultural Engineering, North Carolina State Univ., Raleigh, NC 27606. ORCID: https://orcid.org/0000-0002-5990-8609

[5]Associate Professor, Dept. of Biological and Agricultural Engineering, North Carolina State Univ., Raleigh, NC 27606.

[6]Research Scientist, Dept. of Physical Sciences, Virginia Inst. of Marine Science, Gloucester Point, VA 23062. ORCID: https://orcid.org/0000-0001-7936-1586

Note. This manuscript was submitted on February 21, 2021; approved on April 2, 2022; published online on June 29, 2022. Discussion period open until November 29, 2022; separate discussions must be submitted for individual papers. This paper is part of the ***Journal of Waterway, Port, Coastal, and Ocean Engineering***, © ASCE, ISSN 0733-950X.

(cited between approximately 6% and 15% increase) on the friction angle of soils (Holtz and Gibbs 1956; Kirchner et al. 1990; Yagiz 2001; Antony and Kuhn 2004; Cho et al. 2006; Li et al. 2013; Duncan et al. 2014; Stark et al. 2014). However, changes in friction angles for a mixture of shell and sand particles have not been adequately investigated in the context of their potential role in a bioengineered scour solution. The sediments tested and described in Stark and Wever (2009), Brandes (2011), and Stark et al. (2012) also contained calcium carbonate detritus, but the parent organisms and geomorphological environment of the carbonate material varied considerably from this study. Additionally, the sediment strength testing methodologies and the induced normal stresses differed meaningfully from this study. While particle shape plays an important role, friction angle estimates are also dependent on other compositional and environmental factors that include packing density, gradation, confining pressure, resistance to particle breakage, and biological material present (Duncan et al. 2014; Quiah et al. 2020). Yoon et al. (2010) tested an oyster shell-to-sand mixture ratio of 1:2 (dry weight fraction of about 33%) to develop correlations with friction angles at confining pressures ranging from 40.6 to 162.4 kPa. Friction angles ranged approximately from 50° to 60°. Li et al. (2013) found that granular particle shape plays an important role in friction angles of gravel–clay mixtures. Akin to particle angularity, Li et al. (2013) found that increasing the convexity (a measure of surface roughness) and elongation (a measure of symmetry and roundness) of the granular material in the mixture led to an increase in friction angle on the order of approximately 1°–4°. Yagiz (2001) found that when more than 20% of angular gravel is mixed in with sand, the friction angle increased. The knowledge gaps addressed in this study are: (1) how the presence of relatively small (<5%) weight fractions of oyster shell hash can still influence friction angles; and (2) how the weight distribution of shell hash-sediment mixtures and particle shapes influence sediment shear strength at low confining pressures (<50 kPa) typically found in shallow subtidal and intertidal oyster colony environments. Another purpose for testing at relatively low confining pressures is to limit carbonate shell particles from breaking.

Kirchner et al. (1990) showed that critical shear stress (i.e., minimum flow-induced stress required to entrain and transport sediment particles) is highly dependent on grain protrusion, angle of repose, and grain diameter in relation to the dominant type of bed roughness. Note that friction angle is defined here as the peak effective stress friction angle (which is synonymously used with secant friction angle). When there is no confining pressure and no external load (other than the sediment's self-weight), the secant friction angle is equal to the angle of repose, which is the maximum angle that a pile of coarse-grained sediment is stable at its loosest state (Holtz et al. 2011; Briaud 2013; Stark et al. 2017; Al-Hashemi and Al-Amoudi 2018). Therefore, a higher secant friction angle observed for a shell hash–sand mixture relative to sand only is generally expected to result in the sediment having a higher resistance to erosion. As a result, even if critical shear stress is not directly examined in this study, the influence of oyster shell fragments on friction angle is postulated to provide insights into the benefits of bivalve colonies used to enhance scour mitigation efforts.

This paper presents the findings from several vacuum triaxial tests conducted on sediment samples containing varying amounts of silica-rich sand and shell hash collected from two field sites. Shell hash was identified, measured, and removed from specimens by dissolving carbonates using hydrochloric acid. The field sites were located near an artificial subtidal oyster reef in the Piankatank River in Virginia, USA and natural intertidal oyster reefs in the Rachel Carson Reserve in North Carolina, USA. Field measurements from a portable free-fall penetrometer were also used to estimate friction angles under in situ conditions.

Regional Context

The first field site is in the Piankatank River (PR) in Virginia and the second is in the Rachel Carson Reserve (RCR) in North Carolina [Fig. 1(a)]. The water levels at both sites are affected by semidiurnal tides (NOAA 2018). The PR oyster reef of interest is in the subtidal zone (i.e., always submerged), while the RCR oyster reefs are located in the intertidal zone (i.e., exposed during low tide and submerged during high tide). The species dominant at both sites is the American eastern oyster (*Crassostrea virginica)* (Galtsoff 1964).

Piankatank River Site

The PR is an estuarine river, located west of the Chesapeake Bay. The substrate material for the oysters near the study area consists of oyster rock (granite riprap), shell, mud, and sand (Harding et al. 2010). Due to the overharvesting of natural oyster populations since the early 1900s, research activities and oyster restoration efforts by the Virginia Institute of Marine Science, the US Army Corps of Engineers, and other stakeholders have taken place since the 1990s (Lipcius et al. 2010; Bloodgood 2017, 2019; Consolvo et al. 2020a). Restoration efforts have included the placement of granite riprap-sized stones from barges to create artificial oyster habitats in the PR (Bloodgood 2017).

As shown in Fig. 1(b), there were six field instrument deployment locations—PR1 through PR6—that were within and adjacent to an artificial oyster reef on top of rocks within a sand bed. Based on the local geology and previously reported abundance of natural oyster reefs near PR1 through PR6, the source of the carbonate-based bed material is likely limited to fine shell fragments from oysters and other mollusks (Haven et al. 1981; Harding et al. 2010). The subject oyster reef is under water at depths ranging

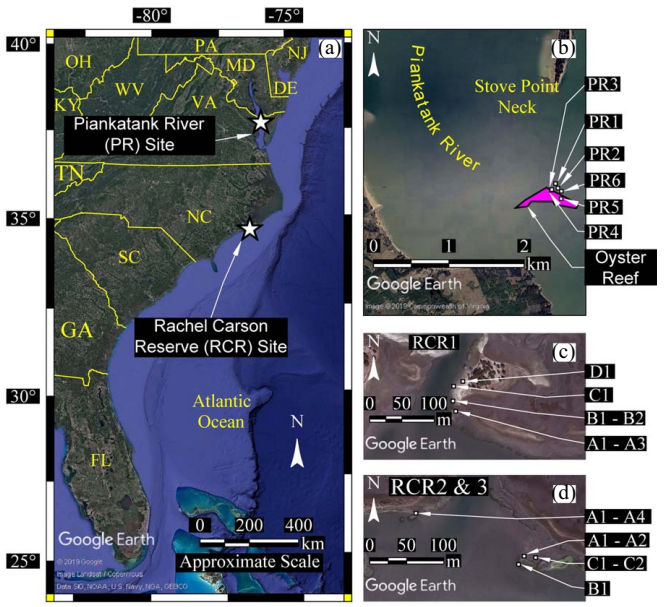

Fig. 1. (Color) Annotated satellite images of the field locations of (a) the east coast of the U.S. (image ©2019 Google, image Landsat/Copernicus, data SIO, NOAA, U.S. Navy, NGA, GEBCO); (b) the Piankatank River near its mouth (image © Google ©2019 Commonwealth of Virginia); (c) the western portion of the Rachel Carson Reserve (subsite RCR1) (image ©Google Earth); and (d) the eastern portion of the Rachel Carson Reserve (subsites RCR2 and RCR3) (image ©Google Earth).

from approximately 2.5–3.5 m based on the Mean Lower Low Water (MLLW) tidal datum (NOAA 2018). Relevant field instruments used at the PR were a Ponar grab sampler and a portable free-fall penetrometer (PFFP). Acoustic Doppler current profiler (ADCP) measurements performed during the field survey showed that depth-averaged flow velocity was on the order of 0.20 m/s on October 4, 2018 during the late morning ebb tide.

Rachel Carson Reserve Site

The RCR intertidal site is located east of Morehead City and south of the Town of Beaufort (NC DEQ 2020). Surrounding rivers and inlet flows influence the water and sediment dynamics around the islands, channels, and shoals that form the RCR (NC DEQ 2020). This coastal environment supports the natural growth of oyster reefs (Delgado 2019). Surficial soils of the RCR are characterized by soft mud, sandy bottoms, shell bottoms, dredge spoil beaches, tidal flats, oyster reefs, salt marshes, maritime forests, and submerged aquatic vegetation (Delgado 2019).

In Figs. 1(c and d), three main subsites are identified—RCR1 through RCR3—where field measurements were taken. Furthermore, within each subsite, multiple sampling locations were selected (tertiary level) for different positions relative to the natural oyster reefs on top of beach sand. The subsites were selected for the known presence of oyster reefs, accessibility, and variations in the local hydrodynamic conditions. RCR1 was exposed to moderate flow conditions, located parallel to the dominant flow, whereas RCR2 and RCR3 were directly exposed to more pronounced flow conditions. Shovels (used to collect grab samples), core tubes (used to collect cylindrical core samples), an X-ray corer (used to capture sediment cross-sections), digital cameras, and a PFFP were utilized in the RCR field survey. With the abundance of oyster colonies observed in the immediate vicinity of the RCR sampling locations [Figs. 1(c and d)], the source of the carbonate-based bed material is also predominantly limited to oyster shell fragments.

From ADCP measurements performed during the field survey, depth-averaged flow velocities at RCR1 were less than 0.10 m/s on July 29, 2019 during the evening high tide. For RCR2 and RCR3, depth-averaged flow velocities on the order of 0.20 m/s were measured on July 30, 2019 during the morning high tide. The tidal range for the evening tide on July 29th was approximately 1.2 m, and the tidal range for the morning tide on July 30th was approximately 0.9 m (NOAA 2019).

Methodology

Field Measurements

The field surveys performed at the PR and RCR were considered exploratory within the context of pursuing the first geotechnical insights into bivalve-sediment interactions. Field measurements were not replicated at both sites because the oyster reef at the PR was submerged and the reefs at the RCR were not at the time of the field surveys, and the substrate conditions were different. Grab sediment samples (disturbed) were collected at all PR and RCR subsites where at least about 2 kg of material was collected at each sample location. At the PR sites, a Ponar grab sampler was deployed from the side of the boat to retrieve sediment samples, and the samples from the RCR were hand-dug during low tide. X-ray cores were taken at nine of the RCR sampling locations (RCR1-A2, -B1, -C2, RCR2-A1, -A3, A4, RCR3-A1, -A2, and -C2) to show the presence of shells in the top 30 cm of the sediment surface. The X-ray corer is approximately 30 cm long by 15 cm wide by 2.5 cm deep plexiglass rectangular prism that can be inserted into the sediment (Massey and Friedrichs 2017).

Overhead photographs of quadrats were taken with a digital camera to estimate the percent area coverage of oyster shells (*QOC*) for all 16 RCR subsites (RCR1-A1, -A2, -A3, -B1, -B2, -C1, -D1, RCR2-A1, -A2, -A3, -A4, RCR3-A1, -A2, -B1, -C1, and -C2). *QOC* is considered a proxy for shell hash content in this study. Thereafter, a 40 × 40 grid (the area of an individual square in the grid is approximately 3.3 cm^2) was overlaid digitally onto the photographs, and squares that visibly contained oyster shells on the surface were colored red, whereas squares that did not have any visible shells were not colored. Green squares were not counted toward the total area because they represent regions where the presence of oyster shells could not be determined. An example is shown in Fig. 2. Note, the quadrat dimensions in the field were 1 × 1 m (made of PVC piping); however, the 40 × 40 grid area had to be smaller (approximately 72 × 72 cm) since the overhead photographs were not perfectly aligned or centered with the quadrats. In the case of Fig. 2, the green squares are where the base of a mini jet erosion test (JET) device (Wardinski et al. 2018) was located, which likely did not have oyster shells present but could not be verified visually afterward from the photographs. The purpose of processing the quadrat overhead photographs was twofold: (1) to contextualize the particle-size distribution data from the RCR presented in this study; and (2) to see if shell coverage is correlated with erodibility parameters estimated from JETs (not within the scope of this paper). Overhead photographs for estimating *QOC* were only collected at the RCR sites. The available equipment was unsuitable for application on the rock-based and submerged oyster reefs in the PR.

A PFFP was utilized for in situ assessment of surficial sediment strength at both field sites; however, only PFFP data from the PR was processed, specifically at Subsites PR1 through PR3. The PFFP deployment locations approximately coincided with the sampling locations. However, the PFFP deployment locations at the RCR site were at least 27 m away from the sampling locations due to site access limitations with a boat from the shallow waters. Therefore, PFFP results are not considered for the RCR site.

The PFFP instrument used was the *blueDrop* by Blue C Designs. It was hand-deployed off the side of a vessel and fell freely from a near-vertical position under its own weight until impact with the seabed. The purpose of deploying the PFFP was to rapidly characterize the seafloor sediments that contain shell hash (Stark and Wever 2009). The probe continuously measures the deceleration

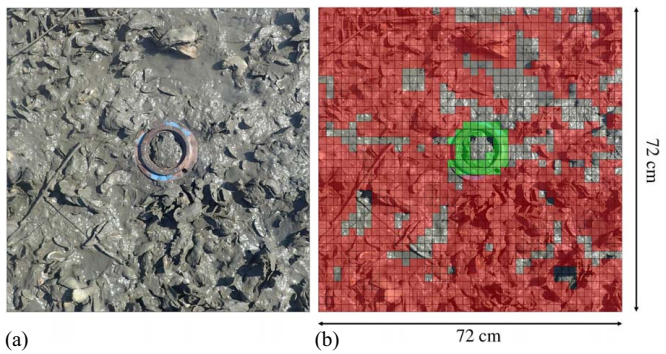

Fig. 2. (Color) Example of an (a) unprocessed and a; and (b) processed overhead quadrat image of how the percent oyster coverage in a quadrat was estimated via a grid pattern for Site RCR1-A1. The *QOC* in this example is approximately 82%.

using five vertical accelerometers ranging from 2 to 250 g, and two 55 g horizontal accelerometers to detect tilt (where g is the acceleration due to gravity) (Blue C Designs 2015). The data sampling rate of the probe is 2 kHz which can produce a displacement resolution better than 1 cm. In situ friction angles (ϕ'_{PFFP}) were estimated from the PFFP deceleration data using the methodology described in Albatal et al. (2020). This procedure involved deriving quasi-static bearing capacity (qsbc) based off the bearing capacity theory from Durgunoglu and Mitchell (1973) for quasi-static cone penetration resistance of soils (Stark et al. 2009, 2012). The derivation of qsbc uses Newton's 2nd Law to estimate the sediment resistance force established from the deceleration data, then divides this force by the product of the penetrated area of the cone and a strain rate correction factor, K. The value of K chosen for this study was 1.25 based on similarities with previous literature in terms of particle-size distributions and the type of PFFP probe used (Stoll et al. 2007; Stark et al. 2012; Albatal et al. 2020). Field relative densities, $D_{r,PFFP}$, were found using a correlation ($D_{r,PFFP} = -2.18 \times 10^{-4} a_{dec}^3 + 1.29 \times 10^{-2} a_{dec}^2 + 1.61 a_{dec} - 13.09$) developed by Albatal et al. (2020) with the PFFP maximum deceleration (a_{dec}) field data for this study. It should be noted, however, $D_{r,PFFP}$ was developed for using a locally sourced quartz sand of specific grain size and range with no mention of shell material present (Albatal et al. 2020). This means that this method in the current form may overestimate $D_{r,PFFP}$ for sands featuring shell hash by associating a stronger sediment resistance (i.e., higher a_{dec}) against the PFFP with an increase in density instead of an increase in frictional resistance from sharper particle shapes.

Laboratory Testing

All acid-treated and nonacid-treated samples from the PR and RCR were classified using the Unified Soil Classification System (USCS) per ASTM D2487 (ASTM 2017a) based on the gradation testing (ASTM D6913; ASTM 2017b) performed on all samples. Before the samples were acid-treated, shell hash particles larger than 2 mm (retained on a No. 10 sieve) were removed, and gradation tests were completed for the retained shell hash portion. Subsequently, the smaller (<2 mm) shell hash that could not be isolated easily from the noncarbonate sand particles were treated with acid. The weight of the smaller-sized shell hash fraction was estimated by weighing the sample before and after treatment with HCl.

To differentiate shell hash contribution to sediment properties, two of the samples from the PR (PR2 and PR6) were treated with hydrochloric acid (HCl) to dissolve carbonate material. This process was intended to retain the nondissolvable, noncarbonate sands in the original samples assumed (no mineralogical testing performed) to be silica-rich quartz minerals, which are generally regarded as inert (Crundwell 2017). While it cannot be proven that indeed all dissolved carbonate materials represented oyster shell hash, local geology and the proximity to the oyster reefs suggests that contributions from other carbonate detritus are negligible.

The dissolution of the carbonate material allowed strength testing to compare samples with and without shell hash. Modified from the rinse method described by Brodie et al. (2011), the HCl was added to the preweighed and predried sediment sample saturated with enough distilled water to dilute the acid to between 3.7 and 4.0 M [a concentration of 1.0 M was effectively used by Komada et al. (2008)]. Thereafter, the diluted acid-sediment mixture was stirred and shaken for approximately two minutes, and then left in a fume hood for at least 12 hours. This allowed enough time for the acid reactions to dissolve the carbonate material in the samples. This duration was found to be adequate for the effervescence to no longer be detected by visual inspection, in line with Komada et al. (2008). The acid-treated sample was carefully poured into a funnel through two stacked ordinary coffee filters. Then, it was rinsed with distilled water until the outflow tested neutral with pH paper. Finally, the sample was redried in an oven at 110°C ± 5°C for at least 12 hours and weighed to estimate the amount of shell hash dissolved. Laboratory limitations and time constrictions hampered the ability to repeat the same elaborate acid-treatment program on the RCR samples. While this would certainly be interesting and is planned for future efforts, it did not affect the results of this exploratory study and is to some degree provided by the photograph estimates of QOC.

The particle-regularity procedure detailed in Cho et al. (2006) was followed to quantify particle shape, which was then used to estimate relative density, $D_{r,cho}$. Samples from Subsites PR2 (nonacid-treated portion of sample), PR6 (acid-treated portion of sample), RCR1-A3, RCR2-A3, and RCR3-C were photographed for this procedure. Instead of using a stereomicroscope as described in Cho et al. (2006), a Sony Alpha a6000 mirrorless digital camera was used to photograph sediment and shell hash particles retained in Sieves nos. 10, 20, and 60. With limited sample sizes able to be collected from the field, the same sample material was used for the particle regularity photographs, the vacuum triaxial tests, and the gradation testing previously performed. For each photograph, three arbitrarily selected individual particles from the retained material on each sieve were examined optically. Thereafter, roundness (R) and sphericity (S) were estimated, which are required to calculate particle regularity ($\rho = (R + S)/2$). R, S, and ρ can range between dimensionless values of 0.1–0.9, and a lower value of ρ for a particle means that it is more angular and less spherical relative to a round and smooth particle (Cho et al. 2006). The reasons for estimating ρ for nonacid-treated and acid-treated samples were to quantify the difference in particle shapes for sediment with and without shell hash and to empirically estimate $D_{r,cho}$. Values of ρ for nonacid-treated samples were expected to be less than acid-treated material because the shell fragments were visually more angular than the noncarbonate sand collected.

Subsequently, maximum and minimum void ratios (e_{max} and e_{min}, respectively) were empirically calculated based on correlations with ρ from Cho et al. (2006), provided the material was <5% fines by weight and had a coefficient of uniformity, $C_u \leq 2.5$ after Youd (1973) [$C_u = D_{60}/D_{10}$, where D_{60} and D_{10} are the particle diameters corresponding to 60% and 10% passing (ordinate) on the particle-size distribution curve per ASTM D2487; ASTM 2017a]. Fig. 3 depicts the photographic analysis and formulaic procedure to estimate $D_{r,cho}$. $D_{r,cho}$ is based on the general definition of relative density ($D_r = (e_{max} - e)/(e_{max} - e_{min})$), where e_{max} and e_{min} are empirically derived, and the void ratio, e, is estimated from multiple specimen measurements of the initial height, diameter, and dry weight as part of the vacuum triaxial test procedure. Note, these initial physical measurements occurred prior to each vacuum triaxial test with the preselected vacuum pressure already being applied to the specimens.

The definition of the variables shown in Figs. 3(a and b) are as follows: r_{max-in} = radius of the largest inscribed circle of the particle; $r_{min-cir}$ = radius of the smallest circumscribed circle of the particle; r_i = radius of curvature at a corner of a particle; N = number of corners examined for one particle; n = number of retained particles examined for a particular sieve; and P_i = percent (by weight) of particles retained on the subject sieve; and the subscript, i, refers to the ith value of the variable in a list of numbers of length n or N.

No bulk samples large enough were collected to perform e_{min} and e_{max} tests (ASTM D4253; ASTM 2016a and D4254; ASTM 2016b, respectively) in this study. The sediments near the oyster

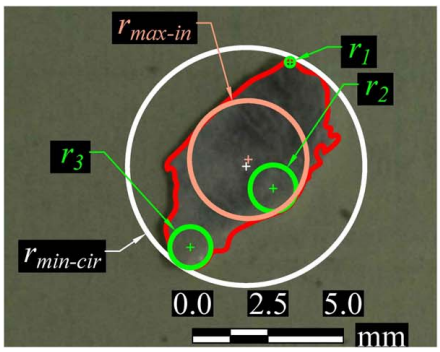

(a)

(b)

1. $S_i = \frac{r_{max\ -in}}{r_{min\ -cir}}$

2. $R_i = \frac{\sum r_i / N}{r_{max\ -in}}$

3. $\rho_i = \frac{S+R}{2}$

4. $\rho_{sieve\ i} = \frac{\sum \rho_i}{n}$

5. $\rho_{sample} = \frac{\sum(\rho_{sieve\ i} \cdot P_i)}{100\%}$

6. $e_{max} \cong 1.5 - 0.82 \cdot \rho_{sample}$

7. $e_{min} \cong 0.9 - 0.44 \cdot \rho_{sample}$

8. $D_{r,cho} = \frac{e_{max} - e}{e_{max} - e_{min}} \times 100\%$

Fig. 3. (Color) (a) An annotated photograph of a single shell fragment (i.e., particle of shell hash); and (b) the formulaic procedure used to estimate $D_{r,cho}$ developed for this study based on information presented in Cho et al. (2006) and Youd (1973).

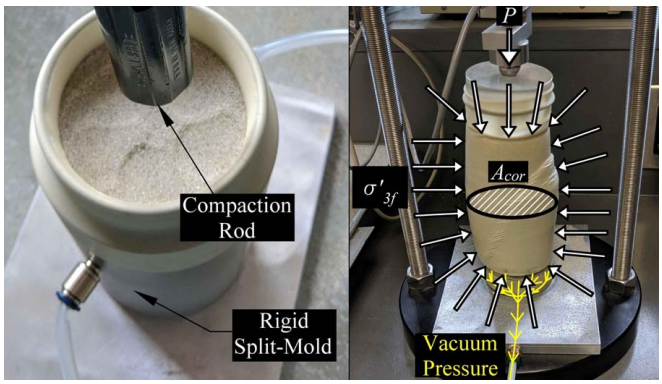

(a) (b)

Fig. 4. (Color) Annotated photographs of (a) a specimen being prepared for a vacuum triaxial test for PR2 (acid-treated); and (b) an ongoing test for PR2 (acid-treated).

reef surveyed at the PR were all coarse-grained in size and did not have cohesion between particles, which made it difficult to effectively retrieve sediment samples with the Ponar grab sampler used. As the samples were being lifted from the side of the boat, the sediments often fluidized and poured out of the small gaps between the clamps of the Ponar grab sampler. This meant several attempts had to be made before a sediment sample of reasonable weight (>2 kg) could be successfully collected. At the RCR, sampling was kept to a minimum to limit the amount of disturbance to the nature preserve managed by the NC DEQ. For the reasons aforementioned and the fact that these surveys were exploratory in nature, a limited number and volume of sediment samples could be taken.

Two other parameters were used to estimate the packing density of the samples: (1) relative density ($D_{r,\text{spher}} \cong (e_{\text{max,spher}} - e)/(e_{\text{max,spher}} - e_{\text{min,spher}})$) assuming idealized packing of spherical and uniformly sized grains in accordance with Cubrinovski and Ishihara (2002), where $e_{\text{max,spher}} \cong 0.91$, $e_{\text{min,spher}} \cong 0.35$, and e is the same as used in calculating $D_{r,cho}$; and (2) the theoretical relative compaction (RC_t) which is a special case of relative compaction (RC). RC is defined as the ratio of the dry unit weight (γ_d) to the maximum dry unit weight ($\gamma_{d\ \text{max}}$) of a soil (Han 2015), where $\gamma_{d\ \text{max}}$ is often estimated from a standard or modified proctor test (ASTM D698; ASTM 2012b or ASTM D1557; ASTM 2012a, respectively). For compaction testing, RC can be more readily field-estimated than relative density (Duncan et al. 2014). However, the authors in this paper propose using RC_t [Eq. (1)] in connection with the laboratory strength results, instead of RC, where γ_s is the maximum theoretical dry unit weight (zero voids) of a soil that can solely be estimated from a specific gravity, G_s, test or the initial void ratio with no laboratory proctor tests needed. G_s tests were performed in accordance with ASTM D854 (ASTM 2014) by a commercial geotechnical laboratory on three samples (nonacid treated sample portions of PR2, PR6, and RCR2-C1), which had already gone through sieve analysis testing.

$$\text{RC}_t = \frac{\gamma_d}{\gamma_s} \tag{1}$$

The laboratory strength results were estimated by performing a total of 29 vacuum triaxial tests (Fig. 4) on PR1 (no acid treatment), PR2 (before and after acid treatment), PR6 (before and after acid treatment), RCR1-A3, RCR2-A3, and RCR3-C1. The samples that were selected for vacuum triaxial testing represented different geomorphological areas at both the PR and the RCR. For instance, PR6 is closer to the oyster reef than PR1, and RCR1-A3, RCR2-A3, and RCR3-C1 are exposed to different local flow regimes. With no ASTM standard for vacuum triaxial testing, the procedure followed Albatal et al. (2020) without the use of the sand raining system. The raining system was not used because the shell material clogged the openings in the diffuser section as this method was not developed for angular shell material. The predried samples were compacted with a rod about 2 cm in diameter [Fig. 4(a)] and compacted into a thin (membrane thickness, $t_m =$ 0.15 mm) triaxial air-tight membrane enclosed by a rigid split-mold. Note, only RCR samples with $QOC < 10\%$ were selected to reduce the possibility of shell fragments puncturing through the thin membrane during vacuum triaxial testing. Before any sediment was placed, the preselected vacuum pressure was applied between the membrane and the rigid split-mold to ensure the membrane was tight up against the rigid split-mold so there would not be folds in the membrane during sediment placement and compaction. Once enough material had been placed and compacted, it was carefully screened off flush with the top of the split mold to a specimen height of approximately 152 mm for each test. The level of compaction effort and number of layers varied depending on the desired packing density; the compaction procedures are detailed in the individual test workbooks available in Consolvo et al. (2020b). The packing densities of the prepared specimens ranged between $19.7\% \le D_{r,cho} \le 90.8\%$, $8.6\% \le D_{r,\text{spher}} \le 51.6\%$, and $53.7\% \le \text{RC}_t \le 61.7\%$. Generally, the intent was to achieve broad ranges of relative densities to simulate a variety of potential field conditions, namely 0%–25%, 25%–50%, 50%–75%, and 75%–100%. A cylindrical cap was then carefully placed on top

of the sediment, then the preselected vacuum pressure was quickly applied to the interior of the membrane through the bottom plate as shown in Fig. 4(b). Right after the vacuum pressure was swiftly switched to the interior of the membrane, the top of the membrane was rolled over the perimeter of the cylindrical cap, then a rubber o-ring was placed over the membrane in a preset groove to seal the triaxial sample. This seal allowed for the vacuum pressure to stabilize to the preselected isotropic confining pressure for the entire testing duration. The split mold was then carefully removed, and the initial diameter of the specimen was measured with a digital caliper at the top, middle, and bottom, and then averaged. The average initial diameters ranged from 67.6 to 72.5 mm. Triaxial confining pressures were set between 2.1 and 49.0 kPa to simulate subtidal and intertidal aquatic conditions. Multiple triaxial tests (at least two—refer to Table 3) were performed on each sample at about the same packing density and at three different confining pressures to estimate shear strength parameters a and b (defined subsequently in this section) per Duncan et al. (2014). The tests were then started where the incremental load applied onto the triaxial sample (P) is generated from the GeoJack Loading instrument, and the confining pressure ($\sigma'_{3f} = \sigma'_3$) is created from vacuum suction controlled with a regulator [Fig. 4(b)]. The maximum variation in the confining pressure allowed during the tests was approximately ±0.5 kPa. Once the deviator stress (σ_d) peaked and started to steadily decline, the tests were then stopped.

The parabolic area correction formula ($A_{cor} = A_0\left[-\frac{1}{4} + \left(\left(\sqrt{25 - 20\varepsilon - 5\varepsilon^2}\right)/4(1-\varepsilon)\right)\right]^2$; Mulabdic 1993) was used to compute the deviator stress ($\sigma_d = P/A_{cor} - \sigma_{dm}$) throughout the test, where A_0 is the initial cross-sectional area, ε is the axial strain, and σ_{dm} is subtracted to account for the added resistance of the rubber membrane ($\sigma_{dm} = (4E_m t_m \varepsilon)/\sqrt{4A_{cor}/\pi}$; where E_m = Young's modulus for the membrane material; ASTM D4767; ASTM 2011). Once the deviator stress could be computed, two approaches were then taken to quantify sediment strength: (1) the secant friction angle (ϕ_{sec}) based on the Mohr-Coulomb failure criterion; and (2) shear strength (τ) using nonlinear strength envelopes.

In order to estimate ϕ'_{sec}, the major and minor principal stresses at failure, σ'_{1f} and σ'_{3f}, respectively, needed to be calculated first. σ'_{3f} was kept constant throughout each test and is the same as the confining pressure (σ'_3). σ'_{1f} is defined in Eq. (2), which is a function of σ'_{3f} and σ_d. The maximum σ_d for each vacuum triaxial test defined specimen failure for this study. Example stress–strain curves, as well as strength results, are provided in Fig. 5, where peak deviator stresses fall between 3% and 6% strain in Fig. 5(a). Thereafter, ϕ'_{sec} was estimated based on Eq. (3) taken from Duncan et al. (2014), which defines the angle between the abscissa and the line tangent to Mohr's circle passing through the origin (no cohesion assumed).

$$\sigma_d = \sigma'_{1f} - \sigma'_{3f} \Rightarrow \sigma'_{1f} = \sigma_d + \sigma'_{3f} \tag{2}$$

$$\phi'_{sec} = 2\left[\left(\tan^{-1}\sqrt{\frac{\sigma'_{1f}}{\sigma'_{3f}}}\right) - 45^\circ\right] \tag{3}$$

As suggested by De Mello (1977) and presented in Duncan et al. (2014), shear strength envelopes can be curved for granular materials, which is applicable to the material sampled in this study. The equation for τ in the form of a power equation (Lade 2010), defined in Eq. (4), was used for this study, which incorporates dimensionless curve-fitting parameters a and b. p_a is the atmospheric pressure (101.3 kPa used in this study), and σ'_N is the effective normal stress on the failure plane [Eq. (5)]. The procedure shown in Fig. 5(b) was followed by Duncan et al. (2014).

$$\tau = ap_a\left(\frac{\sigma'_N}{p_a}\right)^b \tag{4}$$

$$\sigma'_N = 2\sigma'_{3f}\sin^2\left(45^\circ + \frac{\phi'_{sec}}{2}\right) \tag{5}$$

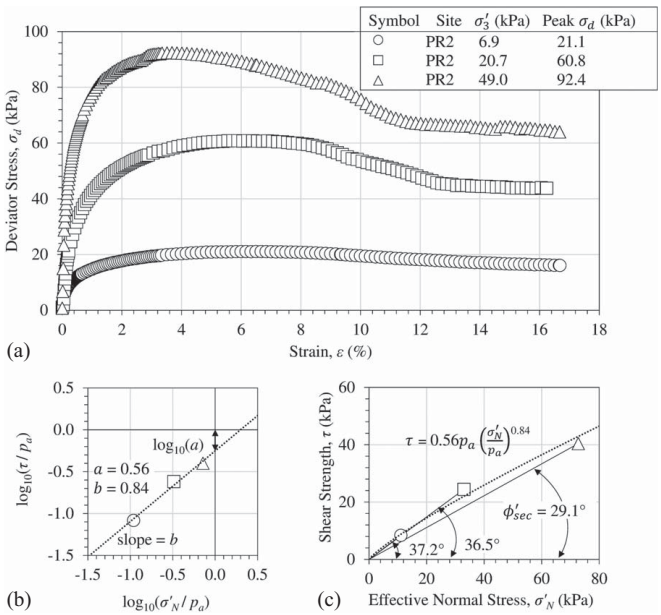

Fig. 5. Example of how ϕ'_{sec} and curve-fitting parameters a and b were estimated from vacuum triaxial tests for subsite PR2 (after acid treatment) corresponding to Group No. 4: (a) stress–strain curve; (b) equal-axis plot to estimate a and b per Duncan et al. (2014); and (c) equal-axis plot showing linear (solid lines) and nonlinear (dotted curve) shear strength envelope interpretations.

Results

Particle-Size Distribution

USCS classifications, the range of median grain sizes (D_{50}), the range of coefficients of uniformity (C_u), the range of coefficients of curvature (C_c), and the range of weight fraction percentages of shell hash from PR and RCR samples are summarized in Table 1. C_u for both sites (PR and RCR) was consistently less than 6—except for one outlier value of 36.40 (sample location: RCR1-B1)—which is the cut off between poorly graded and well-graded sediments (ASTM D2484; ASTM 2017a). The average D_{50} for all samples from the PR and the RCR was approximately 0.28 mm. The sediment USCS classifications from this study for the PR samples generally agree with the findings of Haven et al. (1981) near the subject oyster reef investigated. The sediment classifications from this study for the RCR samples agree with the findings of Delgado (2019).

The particle-size distribution curves for the PR and RCR samples are shown in Figs. 6(a–d). The particle-size distribution curves from the PR are more closely spaced than the ones from the RCR. The standard deviations of C_u for the PR and RCR samples are approximately 0.11 and 1.12 (if RCR1-B1 is excluded), respectively. One reason for the differences in standard deviation is the range of shell hash content was greater for the RCR samples based on QOC estimations. In Fig. 6(b), the shell hash only curves are cut off at a particle size (abscissa) less than 2 mm because the small-sized shell

Table 1. Selected index properties of the samples collected at the RCR and PR

Site	USCS classification(s)	Range of D_{50} (mm)	Range of C_u	Range of C_c	Range of weight fraction of shell hash
PR	SP	0.28–0.32	1.48–1.82	0.96–1.23	3.3%–3.8%[a]
RCR	SP, SP-SM, and SM	0.17–1.09	1.46–36.40[b]	0.54–1.35	Not acid-treated

Note: Index property data for each sample can be found in the associated online data repository (Consolvo et al. 2020b).
[a]This range is based on Samples PR2 and PR6.
[b]36.40 is considered an outlier because it is approximately 3.8 standard deviations away from the mean.

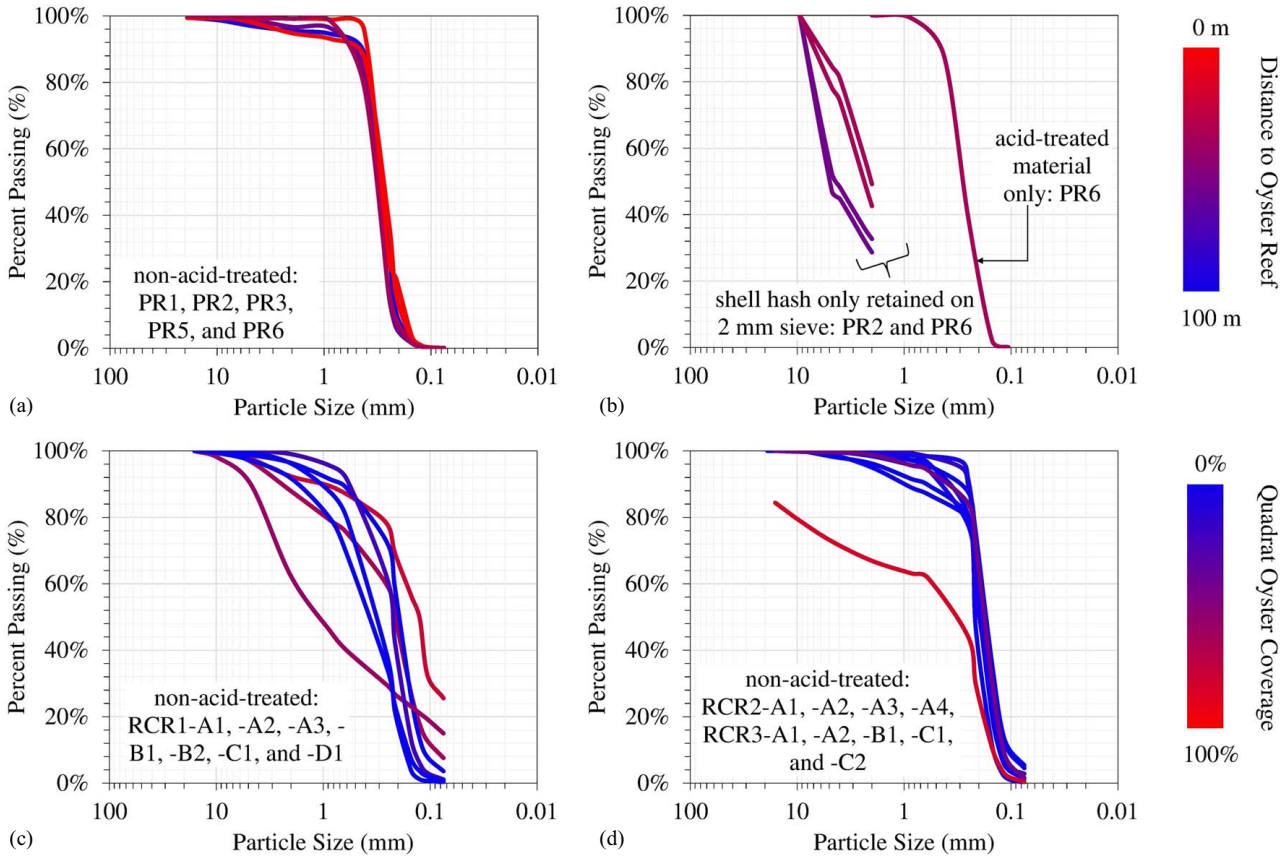

Fig. 6. (Color) Particle-size distribution curves of (a) nonacid-treated PR samples; (b) shell hash only retained on 2 mm sieve and acid-treated material only PR samples; (c) RCR1 samples; and (d) RCR2 and RCR3 samples. Each curve is plotted on a red to blue color scale according to the distance from the oyster reef, x, for the PR samples and the QOC for the RCR samples. QOC and x are considered proxies for shell hash content where curves that are redder likely contain greater amounts of shell material.

material (<2 mm) could not be effectively isolated from the noncarbonate sand particles before selected samples were acid-treated. Therefore, only the weights from before and after acid treatment are known for the small-sized shell material.

More widely distributed particle size ranges were expected, and generally observed (Fig. 6) for samples that had a relatively high shell hash content. This was expected because the shell hash material collected was generally larger in size, and the noncarbonate sands were fairly uniform and smaller in size from initial field observations. The wider distribution curves can be characterized by higher C_u. As shown in Fig. 7, C_u generally decreases the further away from the PR oyster reef and with lower QOC RCR estimations, indicating a greater range in particle sizes with increasing shell hash content.

Friction Angle

ϕ'_{sec} roughly increased with increasing $D_{r,spher}$, $D_{r,cho}$, and RC_t for acid-treated and nonacid-treated PR samples as shown in Figs. 8(a–c). The trend is better approximated by linear relationships for the RCR samples [Figs. 8(d–f)]. The RCR samples had a greater percentage by weight of particle sizes larger than 1 mm relative to nonacid-treated PR samples [Figs. 6(a, c, and d)], which may be a contributing factor in the 6.4° increase in ϕ'_{sec}, on average, observed. During the gradation testing, there was noticeably more shell hash visible on the sieves for the RCR, which was confirmed from the particle size distribution results.

There is an approximate average difference of 5.8° for ϕ'_{sec} from nonacid-treated to acid-treated samples. The average ϕ'_{sec} for the acid-treated samples is approximately 30.2° and approximately 36.0° for the nonacid-treated samples (percent increase of approximately 19.2%). The average $D_{r,cho}$ is 48.5% for the acid-treated samples and 53.5% for the nonacid-treated samples, which equates to an approximate percent increase of 9.9%. Contrastingly, the averages of $D_{r,sphere}$ and RC_t decreased slightly when comparing acid-treated to nonacid-treated samples by 0.4% and 0.2%, respectively. Therefore, the increase in ϕ'_{sec} cannot solely be attributed to

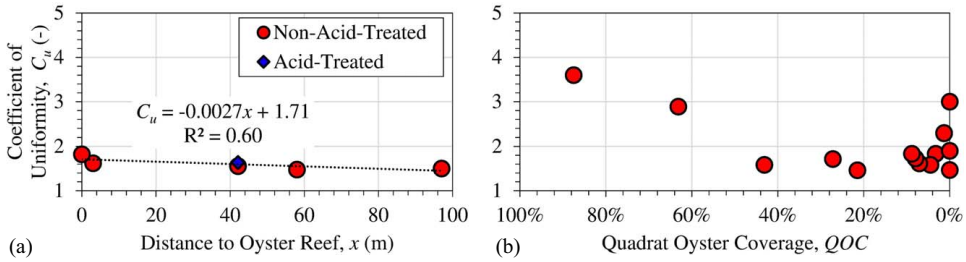

Fig. 7. (Color) Coefficient of uniformity plotted against shell hash content proxy measures for the (a) PR; and (b) RCR. C_u for Sample RCR1-B1 was excluded from the subplot (b) because it was an outlier.

Table 2. Statistical measures for the numerical relationships between friction angle and the listed density parameters

Site	Packing density parameter	Fig.	HCl?	R^2	Linear best-fit equation	p-value	p-value ID
PR	$D_{r,cho}$	8(a)	No	0.40	$\phi'_{sec} = 9.7 \cdot D_{r,cho} + 29.2$	0.03	p-value 1
			Yes	0.44	$\phi'_{sec} = 11.4 \cdot D_{r,cho} + 24.6$	0.05	p-value 2
	$D_{r,\text{spher}}$	8(b)	No	0.40	$\phi'_{sec} = 16.2 \cdot D_{r,\text{spher}} + 29.8$	0.03	p-value 3
			Yes	0.44	$\phi'_{sec} = 19.2 \cdot D_{r,\text{spher}} + 25.1$	0.05	p-value 4
	RC_t	8(c)	No	0.38	$\phi'_{sec} = 88.4 \cdot RC_t - 16.1$	0.03	p-value 5
			Yes	0.45	$\phi'_{sec} = 105.3 \cdot RC_t - 29.7$	0.05	p-value 6
RCR	$D_{r,cho}$	8(e)	No	0.62	$\phi'_{sec} = 47.7 \cdot D_{r,cho} + 7.5$	0.02	p-value 7
	$D_{r,\text{spher}}$	8(d)	No	0.82	$\phi'_{sec} = 101.1 \cdot D_{r,\text{spher}} + 7.4$	0.002	p-value 8
	RC_t	8(f)	No	0.82	$\phi'_{sec} = 547.7 \cdot RC_t - 276.8$	0.002	p-value 9
PR	$D_{r,cho}$	11(a)	No	0.40	$\phi'_{sec} = 9.7 \cdot D_{r,cho} + 29.2$	0.03	p-value 10
	$D_{r,\text{PFFP}}$	11(a)	No	0.086	$\phi'_{\text{PFFP}} = 10.0 \cdot D_{r,\text{PFFP}} + 37.7$	0.3	p-value 11
	$D_{r,cho}$	11(b)	No	0.26	$\phi'_{sec} = -0.060 \cdot x + 37.8$	0.09	p-value 12
	$D_{r,\text{PFFP}}$	11(b)	No	0.0052	$\phi'_{\text{PFFP}} = -0.0053 \cdot x + 43.9$	0.8	p-value 13

increased packing densities between samples. For additional context, the shell hash in the PR2 and PR6 samples accounted for 3.3%–3.8% of their weight. Moreover, the RCR samples with QOC estimations closer to 0% generally had smaller ϕ'_{sec}, except the two data points with the lowest packing density values (RCR2-A3). Note, the upper bound QOC value for the colorbar shown in Fig. 8(e) is a tenth of what was used for the particle-size distribution curves in Figs. 6(c and d) since the QOC values ranged approximately between 0% and 7% for the RCR samples used for vacuum triaxial testing. With the ±0.5 kPa maximum allowed variation in σ'_{3f}, the average ϕ'_{sec} for nonacid-treated and acid-treated samples is 37.8° and 32.0° computed with a low σ'_{3f}, and 34.4° and 28.5° computed with a high σ'_{3f}, respectively. The random error in σ'_{3f} does not appear to alter the increase in friction angle result when shell hash is present either.

The coefficients of determination (also known as R^2, which is the proportion of the variance in ϕ'_{sec} that is predictable from $D_{r,cho}$, $D_{r,\text{spher}}$, or RC_t) and the corresponding best-fit linear equations are tabulated in Table 2. Based on these correlation results, there appears to be no single independent variable (among the three packing density parameters) that clearly predicts the dependent variable (ϕ'_{sec}) better than another. The strongest correlation was expected to be with $D_{r,cho}$ because the particle shape was accounted for in determining the extreme void ratios. However, the average R^2 for $D_{r,cho}$ is 0.48; whereas it is about 0.55 for both $D_{r,\text{spher}}$ and RC_t for the laboratory test results. There is a consistent increase in R^2 from nonacid-treated to acid-treated samples for the PR samples, which may be due to the increased homogeneity in grain size and shape for sediment without shell hash.

To test the statistical validity of whether ϕ'_{sec} is positively correlated with the three packing density parameters for the data in Fig. 8, probability values (p-values) were calculated. p-values can be between 0 and 1, and values closer to 1 are correlations that are more likely to have occurred by random chance (i.e., no statistically significant correlation exists for the given data). Literature (Feinstein 1975; Goodman 2008) customarily recommends statistically significant correlations be limited to p-values ≤ 0.05. In Table 2, p-values range between 0.002 and 1, where p-value 11 through p-value 13 were all greater than 0.05 by about 0.6, on average, indicating the corresponding correlations are not statistically significant. These statistical results merely suggest that the remaining correlations are potentially valid and further experimentation is merited.

Shear Strength

The nonlinear shear strength equation [Eq. (4)] does not appear to estimate τ significantly differently than its linear counterpart, $\tau = \sigma'_N \tan(\phi'_{sec})$, based on the results shown in Fig. 9(a). With b capped at 1.0 for the calculated ordinate values plotted on Figs. 9(a and b), the average absolute difference between the nonlinear and linear estimate of τ is approximately 0.9 kPa, or about 4% of their averages. This difference excludes two nonacid-treated RCR outliers shown in Fig. 9(a). As shown in Table 3, there were only two vacuum triaxial tests successfully performed for Group No. 9 completed at small confining pressures (4.8 and 6.9 kPa). Such limited number of tests most likely resulted in $b \gg 1$ in addition to the small confining pressures. Nevertheless, Fig. 9 reveals computing τ in the form of a nonlinear or linear equation does not yield significantly different results for shell-hash-laden sediment tested at confining pressures between 2.1 and 49.0 kPa.

In Fig. 9(b), τ is predominantly less (i.e., lower shear strength) for the acid-treated samples for a given σ'_N, which is in line with the primary hypothesis of this study. Half of the test groups had values

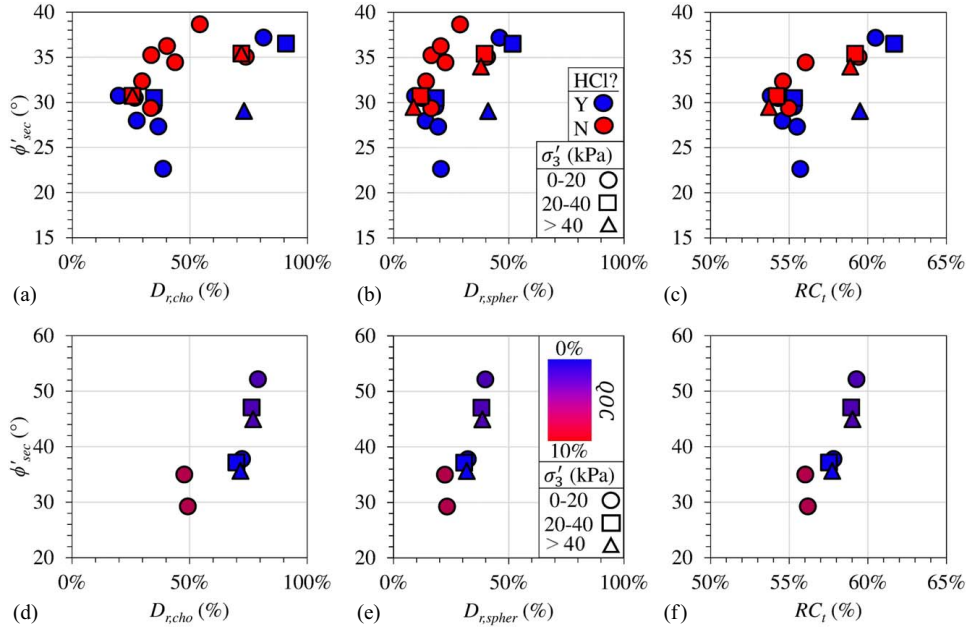

Fig. 8. (Color) Secant friction angles estimated from vacuum triaxial tests are plotted against: (a) $D_{r,cho}$; (b) $D_{r,\text{spher}}$; (c) RC_t on nonacid-treated and acid-treated PR samples; and (d–f) the same variables are plotted for nonacid-treated RCR samples. The legend in (b) is applicable for (a–c), and the legend in (e) is applicable for (d–f).

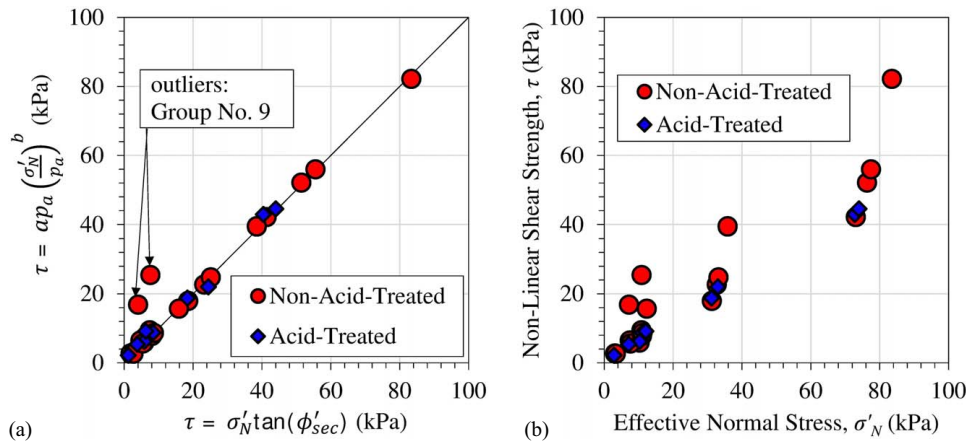

Fig. 9. (Color) (a) Equal-axis plots of shear strength computed from the nonlinear power equation [Eq. (4)] versus from its linear counterpart ($\tau = \sigma'_N \tan(\phi'_{\text{sec}})$); and (b) plot of nonlinearly computed shear strength versus the effective normal stress for all the vacuum triaxial PR and RCR test results. b values were set to 1.0 for calculating τ if they were originally found to be greater than 1.0 for the ordinate values plotted on (a and b).

of $b < 1.0$, indicating nonlinear strength envelopes would appropriately fit the data. When values of $b > 1.0$ were estimated, the data is more appropriately fitted by a linear strength envelope (i.e., b is capped at 1.0). However, considering the low-end variation in σ'_{3f} (−0.5 kPa), all the test groups have a b value less than 1.0, except Group No. 9. Linear strength envelopes were expected for the tests run at relatively small confining pressures (2.1–8.3 kPa), whereas greater degrees of nonlinearity were expected for the larger confining pressures (6.9–49.0 kPa) tested. This was generally observed where the average b value for small confining pressures was greater than 1.0, and 0.95 for the larger confining pressures (Table 3).

Field Results

X-ray cores (approximately 30 cm in length) collected at the RCR indicate that oyster shell fragments were not limited to the surface but were observed down to about 30 cm below the surface. As an example, three X-ray images are shown in Fig. 10, where a relatively large angular oyster shell is revealed in the RCR1-A2 core at a depth of approximately 20 cm below the surface level.

Friction angle estimates based on PFFP field tests performed on shell-hash-laden sediment at PR1–PR3 were used to contextualize the vacuum triaxial laboratory-based friction angle estimates performed on nonacid-treated Samples PR1, PR2, and PR6 (Fig. 11). Since no PFFP tests were conducted at the RCR sample locations, only calculated data from the PR is presented in Fig. 11 (also summarized in Table 3). While the slopes of the linear best-fit lines are similar for ϕ'_{sec} versus $D_{r,cho}$ (9.7) and ϕ'_{PFFP} versus $D_{r,\text{PFFP}}$ (10.0), there is an approximate 9° discrepancy (higher for ϕ'_{PFFP}) between ordinate intercepts per Table 2. $D_{r,\text{PFFP}}$ values were higher by 16%, on average, than the laboratory prepared relative densities ($D_{r,cho}$). In Fig. 11(b), friction angle results are plotted against

Table 3. Sample properties and strength parameter results

Site	Group no.	HCl?	ρ	G_s	$D_{r,cho}$ (%)	σ'_{3f} (kPa)	Linear strength envelope			Nonlinear strength envelope		
							ϕ'_{sec} (°)	ϕ'_{sec} (°) with variations[a] in σ'_{3f}		a and $\boldsymbol{b}$	a and $\boldsymbol{b}$ with variations in σ'_{3f}	
							ϕ'_{sec} (°)	Low σ'_{3f}	High σ'_{3f}	a $\boldsymbol{b}$[b]	Low σ'_{3f}	High σ'_{3f}
PR1	1	No	NT	NT	73.7	6.9	35.1	36.8	33.4	0.68 **0.98**	0.68 **0.95**	0.68 **1.01**
					71.9	20.7	35.4	36.0	34.9			
					69.2	49.0	34.0	34.2	33.7			
	2	No	NT	NT	33.4	6.9	29.4	31.2	27.6	0.58 **1.00**	0.57 **0.97**	0.58 **1.04**
					25.6	20.7	30.7	31.3	30.1			
					20.6	49.0	29.5	29.8	29.2			
PR2	3	No	0.69	2.71	26.6	2.1	30.5	37.1	25.0	0.88 **1.12**	0.66 **0.97**	1.18 **1.28**
					29.6	4.8	32.3	35.0	29.9			
					43.7	6.9	34.4	36.2	32.8			
	4	Yes	NT	NT	81.3	6.9	37.2	38.9	35.6	0.56 **0.84**	0.56 **0.87**	0.56 **0.87**
					90.8	20.7	36.5	37.1	36.0			
					73.0	49.0	29.1	29.3	28.8			
	5	Yes	NT	NT	34.5	6.9	29.5	31.4	27.8	0.60 **1.02**	0.60 **0.99**	0.61 **1.06**
					34.7	20.7	30.5	31.1	29.9			
					19.7	49.0	30.7	31.0	30.5			
PR6	6	No	NT	2.72	54.2	2.1	38.7	44.6	33.7	0.59 **0.91**	0.49 **0.81**	0.71 **1.02**
					33.5	4.8	35.2	37.8	32.9			
					40.2	6.9	36.2	38.0	34.6			
	7	Yes	0.70	NT	38.6	2.1	22.6	29.8	16.8	0.76 **1.16**	0.55 **0.99**	1.12 **1.37**
					27.4	4.8	28.0	30.7	25.5			
					36.5	8.3	27.3	28.9	25.8			
RCR1-A3	8	No	0.65	NT	79.1	6.9	52.2	53.5	50.9	0.96 **0.87**	0.96 **0.85**	0.96 **0.88**
					76.4	20.7	47.1	47.5	46.6			
					77.0	49.0	44.9	45.1	44.7			
RCR2-A3[c]	9	No	0.67	NT	49.3	4.8	44.9	31.9	26.8	2.35 **1.54**	1.93 **1.41**	2.86 **1.67**
					47.8	6.9	29.2	36.7	33.3			
RCR3-C1	10	No	0.62	2.72	72.3	6.9	35.0	39.5	36.2	0.71 **0.96**	0.71 **0.94**	0.72 **0.99**
					69.9	20.7	37.2	37.7	36.6			
					71.6	49.0	35.6	35.9	35.4			

Note: NT = not tested.
[a]$\sigma'_{3f} \pm 0.5$ kPa.
[b]The values for the dimensionless curve-fitting parameter, b, is in boldface within each group. When values of $b > 1.0$ were estimated, the data is more appropriately fitted by a linear strength envelope (i.e., b is capped at 1.0), which is how τ is computed in Figs. 9(a and b).
[c]Only two successful vacuum triaxial tests were able to be performed.

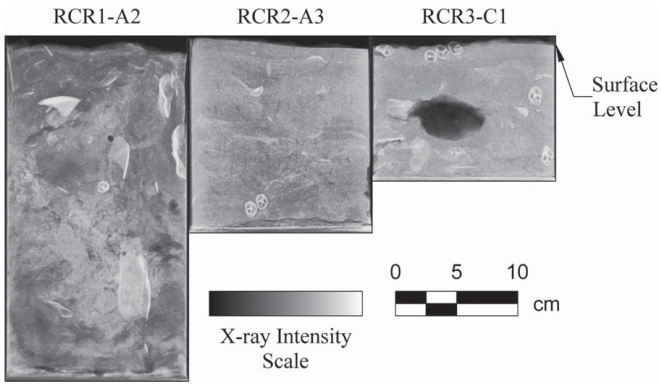

Fig. 10. Three examples of X-ray images (cropped) from three X-ray cores at RCR. Black shades represent low X-ray intensity units (fewer X-ray photons absorbed, i.e., low density, softer, and/or more porous); white shades represent high X-ray intensity units (more X-ray photons absorbed, i.e., higher density, harder, and/or less porous).

distance from the reef, x, in the PR. For both the field and laboratory results in Fig. 11(b), there is a subtle (although, statistically insignificant per Table 2) increase in ϕ'_{sec} and ϕ'_{PFFP} closer to the reef.

Discussion

Particle-Size Distribution

As seen in Fig. 6(b), a wider range of particle sizes is generally observed for shell material only, indicating the sizes of the shells are less uniform than the noncarbonate sand grains. To minimize impacts on the oysters, sampling at the RCR was limited to areas within the quadrats that were not entirely covered with oyster shells but where some sand was exposed. Therefore, the samples collected may not be representative of the highest percentage of shell content present within each of the quadrat RCR sampling locations. Future work should include attempting to correlate *QOC* with shell hash weight fraction to rapidly assess the suitability of

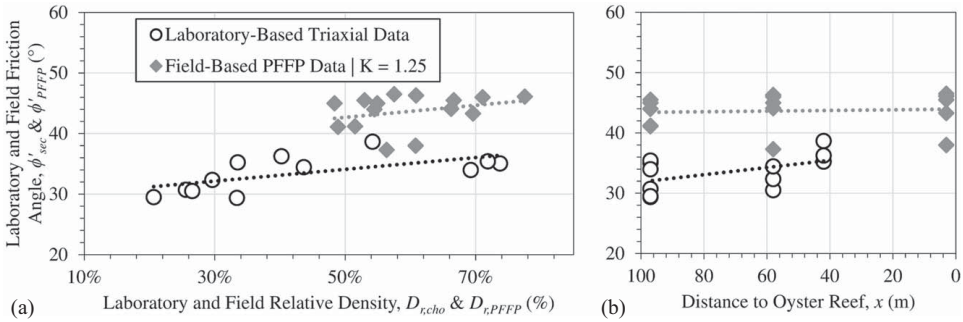

Fig. 11. Field- and laboratory-based friction angle results versus: (a) relative density; and (b) distance to the oyster reef from nonacid-treated PR samples.

an area for scour susceptibility. With respect to geotechnical properties, well-graded particles will generally exhibit a greater resistance to shear for a given normal stress, compared to poorly graded particles (Duncan et al. 2014), which is observed in this study. Provided some level of densification is achieved, the smaller-sized particles tend to fill the voids created from the larger-sized particles, making the sediment mass denser (Lambe and Whitman 1969).

Friction Angle

Much of the literature regarding particle characterization of oyster shells revolves around biochemical applications of shells in a powder form (Kuo et al. 2013). With respect to geotechnical literature, calcareous sands (soil material partially composed of calcium carbonate) are examined more so than shell hash, in general (McDowell and Bolton 2000; Stark et al. 2012; Shahnazari and Rezvani 2013; Ata et al. 2018). However, Yoon et al. (2010) specifically studied the effects of an oyster shell-sand mixture on sediment strength and compressibility. This study similarly showed higher C_u for the oyster shell-sand mixture compared to sand only. The sediment samples Yoon et al. (2010) tested contained large (>10 mm) crushed oyster shell particles (about 33% by dry weight) and contained little to no fine-grained soil particles. In contrast, this study evaluated shear strength for smaller weight fractions of shell hash. It should be noted that differently than in Yoon et al. (2010), shell hash content was estimated here through removal of all carbonate materials which may have contained some carbonate detritus not originating from oysters, although local geology and proximity to the oyster reef suggests that the contribution of carbonate materials is mainly from oysters. Having a broad range of shell hash weight fractions used for friction angle tests is an important aspect toward characterizing the potential positive effects oyster colonies have on their environment with regard to increased resistance to shearing and potential scour mitigation. The average friction angle for Yoon et al. (2010) was roughly 55°, and it was approximately 36.0° in this study for samples with shell hash. While different test methods were used to estimate the shear strength between the two studies, it was expected and generally noted that a higher shell content (weight fraction of shell hash for Yoon et al. (2010) was approximately ten times greater than this study's) should yield higher friction angles.

The increase in secant friction angles observed in the specimens with shell hash relative to specimens without shell hash generally agrees with literature that angular shell particles contribute to an increase in sediment shear strength. Yagiz (2001) demonstrated this with an approximate 6% increase (2°) in friction angle with 10% by weight of angular gravel intermixed with a medium sand (0.2–0.4 mm in size). Unlike Yagiz (2001), with only a presence of approximately 3.5% by weight of angular oyster shell material, the friction angle increases by approximately 19% (~6°) relative to acid-treated samples in this study. This signifies that a low weight fraction percentage (at least 3%) of shell hash can improve the shear strength of sand considerably at low confining pressures. Brandes (2011) generally corroborates these findings, which showed friction angles for calcareous-laden sands were greater than for the quartz-dominated sands by an average of about 23% (~7°).

Cho et al. (2006) showed an increase in the critical state friction angle with decreasing particle regularity, ρ. Critical state friction angle is the point at which the sediment mass strains without further volume change and with a constant σ_d, which can be equivalent to the angle of repose for granular material (Lambe and Whitman 1969; Al-Hashemi and Al-Amoudi 2018). Li et al. (2013) revealed that high surface roughness (i.e., convexity) of gravel particles led to an increase in the friction angle for three different weight fractions (40%, 70%, and 100%) of gravel in a clay-gravel mixture, relative to smooth particles. Stark et al. (2014) showed an approximate 15% increase (5°) in the friction angle with 25% weight fraction of a flat, elongated sand added to round to angular gravel. In this study, the average ρ for specimens with shell hash was approximately 0.66, and without it was approximately 0.70 (increase of approximately 6%), which generally agrees with the trends cited, albeit a smaller range of ρ was found than in Cho et al. (2006). Strictly adhering to the methodology of Cho et al. (2006) in estimating ρ by use of a stereomicroscope could yield greater understanding on the influence shell-hash-laden material has on its friction angle for future research. Additionally, mineralogy testing should be performed to narrow the potential applicability.

The scatter in the secant friction angles as a function of relative densities (Fig. 8) can be attributed to natural variations in the grain mineralogy and uncertainty in the empirical correlations used to estimate e_{max} and e_{min}, which directly affect $D_{r,cho}$. With respect to a published dependence of friction angle of cohesionless soils on relative density ($\phi'_{sec} \cong 14D_r + 28$; estimated graphically for the uniform fine sand line in Figure 18 in Schertmann 1978), the linear best-fit equations from Table 2 that predicted the friction angle to within 3° of the published correlation correspond to the same rows as p-value 1, p-value 4, and p-value 10. While this may seem promising, there were still three correlations (rows corresponding to p-value 6, p-value 8, and p-value 9) that were greater than 10° off, so improvements should be pursued in predicting friction angles from a packing density parameter for shell-hash-laden sediment.

Although Shahnazari and Rezvani (2013) did not perform tests with oyster shell fragments, they did conclude a minimum

confining pressure of approximately 650 kPa (about an order of magnitude greater than the pressures in this study) is required before significant particle breakage of calcareous sands would occur. In Lee and Seed (1967), particle crushing of Sacramento River sand and Ottawa sand (no shell hash materials mentioned) was not readily observed until at least about 1,000 kPa. While no particle crushing was expected with the relatively low confining pressures, some of the more brittle carbonate material could have broken during the preparation of the sample. Samples that were compacted to achieve high relative densities (>50% for this study) may have experienced small amounts of particle crushing. Improvements for future studies should include performing grain size analyses before and after vacuum triaxial testing to verify minimal to no particle breakage is occurring, by following the methodology outlined in Shahnazari and Rezvani (2013).

Acid-treated values of ϕ'_{sec} could also be lower than nonacid-treated because carbonate-based minerals that may have been coating the surface of the noncarbonate sand particles would have dissolved during the acid-treatment process, leading to progressive rounding of sharp edges and subduing irregularities (Margolis and Krinsley 1971; Bullard et al. 2004). Rounded particles typically exhibit a lower resistance to shear (i.e., lower ϕ'_{sec}) than angular particles (Duncan et al. 2014). Future studies could examine the effect of particle rounding on ϕ'_{sec} due to the dissolution of carbonate-based surface coatings on noncarbonate sands by carefully examining individual particles before and after acid treatment with a microscope.

Shear Strength

Confining pressures can be considered small (2.1–49.0 kPa in this study) relative to typical triaxial pressures found in literature, and therefore there were no pronounced nonlinear strength envelopes ($b \ll 1.0$) observed in this study. Half of the values of the strength parameter b were equal to or greater than 1.0, and the remainder were 0.90 on average. With the same a, a higher b will result in a less curved strength envelope (limited to $b \leq 1.0$), relative to a lower b. If the tests had been conducted at a greater range of confining pressures, the estimated values of b would be expected to decrease (Charles and Watts 1980; Charles and Soares 1984; Perry 1994; Lade 2010; Duncan et al. 2014), leading to more pronounced nonlinear relationships between shear strength and effective normal stress. Most likely, the observed slight nonlinearity is caused by dilatancy effects (i.e., tendency for compacted coarse-grained material to expand in volume) (Rowe 1962; Lambe and Whitman 1969), rather than by particle breakage, occurring on the more densely prepared samples. However, slight variations in packing density between triaxial tests within a group could also be contributing to the nonlinear shear strength results. If particle crushing was occurring, the b value for the larger confining pressure tests would be expected to increase and possibly exceed 1.0, which is observed at much greater pressures in Lee and Seed (1967). This is not the case though for this study, so the abnormal values of b greater than 1.0 were likely attributed to instrument error on the regulator governing confining pressure as well as variation in packing density between the samples tested.

Effects of Packing Density

In an attempt to reduce the uncertainty in estimating $D_{r,cho}$, which is based on photographic estimates of ρ and its subsequent correlations with e_{max} and e_{min}, and the somewhat unrealistic spherical particle assumption in estimating $D_{r,spher}$, RC_t was also computed. Furthermore, the range of $D_{r,cho}$ for single test groups varied between 1.5% and 20.7%, meaning consistent densities were not necessarily achieved for each test group when preparing the triaxial samples in the laboratory. D_r may be the same for two different particle packing configurations but may have different shear resistance abilities from the rearrangement potential. However, RC_t was not better in predicting ϕ'_{sec} in that the coefficients of determination for RC_t were about the same, on average, than those for $D_{r,spher}$ or $D_{r,cho}$ (Fig. 8). The initial expectation was that RC_t would more accurately represent the packing density of the prepared samples, and therefore improve predictions of ϕ'_{sec}. The reason for this initial expectation was because RC_t is only a function of the void ratio, e, of the prepared sample [derived in Eq. (6)]. γ_w is the unit weight of water at a standard temperature, γ_d is the dry unit weight (allows for air voids), and γ_s is the unit weight of particle solids (no air voids).

$$RC_t = \frac{\gamma_d}{\gamma_s} = \frac{\left(\frac{G_s\gamma_w}{1+e}\right)}{G_s\gamma_w} \Rightarrow RC_t = \frac{1}{1+e} \tag{6}$$

To reduce the scatter in RC_t, even more care would have to be taken in estimating e and ϕ'_{sec}. This could be done by more accurately measuring the initial specimen volume and how it changes during testing, akin to 3D scanning methods proposed by Hall et al. (2009). However, based on the results in this study, RC_t does not appear to be a useful parameter to predict friction angle alone, nor can void ratio be readily estimated in the field. ϕ'_{sec} is also dependent on confining pressure which would need to be adequately accounted for to potentially reduce scatter. Moreover, future testing should include performing e_{max} and e_{min} testing to improve estimates of relative density. However, the test method in ASTM D4253 (ASTM 2016a) would likely cause particle breakage of the shell hash material leading to artificially low estimates of e_{min}, so thoughtful alternative methods would have to be followed.

Field Measurements

In terms of the PFFP field sediment strength results, the low coefficients of determination for $D_{r,PFFP}$ and x in predicting ϕ'_{PFFP} were expected because the relative density correlation used was developed for sands without shell fragments present. Furthermore, the range of $D_{r,PFFP}$ was smaller than $D_{r,cho}$ by about 24% just for PR samples, which limited the analysis of ϕ'_{PFFP}. Shell hash content—proxied by D_{50} and C_u—did not appear to vary considerably as a function of the distance away from the reef for the PR samples per Figs. 6(a) and 7(a). This further limited the variability present to see changes in ϕ'_{PFFP}. The correlation between ϕ'_{PFFP} and $D_{r,PFFP}$ and x are not statistically significant since the p-values were greater than 0.05 [Table 2, Figs. 11(a and b)], which may be a result of the lack of variability discussed.

Previous investigations have revealed that the bearing capacity method from Durgunoglu and Mitchell's (1973) theory underestimates ϕ'_{PFFP} by approximately 2° (Albatal et al. 2020) compared to laboratory-estimated friction angles (ϕ'_{sec} in this paper). The results in Fig. 11(a) show that the opposite occurrence is observed, where $\phi'_{PFFP} > \phi'_{sec}$ by about 9°. Generally, the choice of strain rate correction factor, K, to ultimately compute ϕ'_{PFFP} could provide an explanation for deviation. A $K = 1.25$ was chosen for this study based on similarities with previous literature (Stoll et al. 2007; Stark et al. 2012) in terms of particle-size distributions, the PFFP probe used, and the bearing capacity method, but future studies should follow a calibration procedure to estimate K and $D_{r,PFFP}$ for the soil type being investigated, especially with shell hash present. K is inversely proportional to ϕ'_{PFFP}; therefore, a higher K (>1.25) used in the analyses would be expected to better align

the field and laboratory results. Doing the analysis with $K = 1.5$ yielded ϕ'_{PFFP} only about 1° less than with $K = 1.25$. Since a value of 1.5 is an upper limit cited in current free-fall penetrometer literature (Stoll et al. 2007; Stark et al. 2012; Stephan et al. 2015; Albatal et al. 2020), the strain rate correction factor is unlikely to explain the discrepancy solely. Without a clear explanation for the 9° discrepancy in friction angles observed, a more focused PFFP investigation is warranted in a sediment environment with varying amounts of shell hash. Future research should also incorporate mineralogical composition testing to narrow the definition of shell hash and the noncarbonate materials present. Nonetheless, the PFFP test results showed (although in a statistically limited fashion) surficial seafloor sediments with shell hash have a higher shear resistance relative to clean quartz sands, which is similarly found in Stark and Wever (2009) as well as in line with Stark et al. (2012) who tested carbonate sand versus quartz sand using a PFFP.

Conclusions

This study pursued geotechnical insights into the influence of bivalve shell fragments on sediment shear strength estimated from laboratory- and field-based methods. It was motivated by the long-term goal of the application of bivalves for scour and erosion protection. Two field investigations that involved sediment sampling and in situ strength measurements from a PFFP were completed where artificial and natural oyster reefs were present. Subsequent laboratory testing was conducted to dissolve carbonate shell material from selected samples and thereafter test their resistance to shear in comparison with samples in which shell fragments remained. Particle sizes ranged from gravel-sized to fine-grained for the samples collected at the two field sites with median grain sizes ranging between 0.17–1.09 mm. The following five conclusions can be drawn:

1. Secant friction angles of specimens tested with shell hash (approximately 3.3%–3.8% by weight) were higher, on average, by approximately 6°, compared to specimens without shells. This indicates a higher resistance to shear for a given load with shell hash present.
2. As expected, specimens prepared at higher relative densities (more compact) for the vacuum triaxial tests generally exhibited higher peak deviator stresses (failure). The three methods for estimating specimen density (relative density assuming idealized uniform spherical particles, relative density based on correlations with particle shape developed by Cho et al. (2006), and theoretical relative compaction based on initial void ratios) were, on average, about the same in their certainty for predicting secant friction angles. The average coefficients of determination for the three methods (in the same order as before) were approximately 0.55, 0.49, and 0.55.
3. Samples that were closer to the oyster reef or had a high percent coverage of oyster shells (a proxy for shell hash content) exhibited less uniform particle-size distributions (i.e., higher coefficient of uniformity). This indicates that carbonate shell particles contributed to the higher coefficients of uniformity estimated from grain-size analyses.
4. Regularities—a function of particle roundness and sphericity—for sediment samples with shell hash were lower, on average, by approximately 0.04 (decrease of approximately 6%) than sediment samples without shells, which could be a contributing factor of the higher sediment shear strengths observed.
5. The friction angle results from the PFFP showed a similar trend with the laboratory-estimated friction angles, albeit with a discrepancy of about 9°. This discrepancy is possibly due to the relative density correlation and the strain rate correction factor not being calibrated with shell-hash-laden material, and the lack of variability in the shell hash content between the samples collected at the Piankatank River site. Therefore, a more focused investigation should generate correlations between friction angle and packing density parameters with PFFP data in a shell-hash-rich setting accompanied by mineralogy testing.

Further investigations should involve careful laboratory testing to estimate the minimum and maximum void ratios of sediments with varying amounts (by weight) of shell fragments intermixed. This would produce a higher reliability of the relative densities and may improve the correlation between relative density and secant friction angle for sands with shell fragments. The results presented herein confirmed the findings of previous literature that particle shape plays an important role in shear strength. This study expanded the domain of sediment types and confining pressures for shear strength testing on sand with low percentages of shell hash.

Addressing the influence oyster colonies have on the erodibility of sediments should also be investigated through field and laboratory efforts as a continuation of this study. Future efforts should consider the important role friction angles have on erosion and use the findings from this paper to study spatiotemporal variations in scour near estuarine and marine areas of interest that could accommodate bivalve farms. Refined interpretation of PFFP tests in sediment environments containing shell hash in combination with long-term sediment transport monitoring near oyster reefs could yield further understanding and bring the goal of using bivalves as a bioengineered soil improvement solution closer to implementation.

Data Availability Statement

All data, models, and code generated or used during the study are available in a repository or online in accordance with funder data retention policies (Consolvo et al. 2020b).

Acknowledgments

The authors acknowledge funding from the National Science Foundation through grants CMMI-1820848 and CMMI-1820842. The authors thank Melody Thomas, Liz Smith, Matthew Campbell, Peter Mewis, Julie Paprocki, Paul Richardson, Brandon Puckett, and Paula Gillikin for fieldwork assistance. In addition to the fieldwork help, the authors also thank the graduate students in the coastal and marine geotechnics team and A.J. Prussin at Virginia Tech for laboratory and editorial aid. The authors also acknowledge Bruce Hatcher for helping to review this paper, as well as two anonymous reviewers and the associated editor whose comments contributed to the improvement of this article.

References

Abel, S., C. Bacher, A. Birch, D. C. Brady, A. Breckwoldt, S. B. Bricker, and P. Ermgassen. 2019. *Good and services of marine bivalves*. Cham, Switzerland: Springer.

Albatal, A., N. Stark, and B. Castellanos. 2020. "Estimating in situ relative density and friction angle of nearshore sand from portable free-fall penetrometer tests." *Can. Geotech. J.* 57 (1): 17–31. https://doi.org/10.1139/cgj-2018-0267.

Al-Hashemi, H. M. B., and O. S. B. Al-Amoudi. 2018. "A review on the angle of repose of granular materials." *Powder Technol.* 330 (3–4): 397–417. https://doi.org/10.1016/j.powtec.2018.02.003.

Antony, S. J., and M. R. Kuhn. 2004. "Influence of particle shape on granular contact signatures and shear strength: New insights from simulations." *Int. J. Solids Struct.* 41 (21): 5863–5870. https://doi.org/10.1016/j.ijsolstr.2004.05.067.

Arneson, L. A., L. W. Zevenbergen, P. F. Lagasse, and P. E. Clopper. 2012. *Evaluating scour at bridges*. Publication No. FHWA-HIF-12-003. Washington, DC: Federal Highway Administration.

ASTM. 2011. *Standard test method for consolidated undrained triaxial compression test for cohesive soils*. Designation No. D4767. West Conshohocken, PA: ASTM.

ASTM. 2012a. *Standard test methods for laboratory compaction characteristics of soil using modified effort (56,000 ft-lbf/ft3 (2,700 kN-m/m3))*. Designation No. D1557. West Conshohocken, PA: ASTM.

ASTM. 2012b. *Standard test methods for laboratory compaction characteristics of soil using standard effort (12,400 ft-lbf/ft3 (600 kN-m/m3))*. Designation No. D698. West Conshohocken, PA: ASTM.

ASTM. 2014. *Standard test methods for specific gravity of soil solids by water pycnometer*. Designation No. D854. West Conshohocken, PA: ASTM.

ASTM. 2016a. *Standard test methods for maximum index density and unit weight of soils using a vibratory table*. Designation No. D4253. West Conshohocken, PA: ASTM.

ASTM. 2016b. *Standard test methods for minimum index density and unit weight of soils and calculation of relative density*. Designation No. D4254. West Conshohocken, PA: ASTM.

ASTM. 2017a. *Standard practice for classification of soils for engineering purposes (unified soil classification system)*. Designation No. D2487. West Conshohocken, PA: ASTM.

ASTM. 2017b. *Standard test methods for particle-size distribution (gradation) of soils using sieve analysis*. Designation No. D6913. West Conshohocken, PA: ASTM.

Ata, A., T. N. Salem, and R. Hassan. 2018. "Geotechnical characterization of the calcareous sand in northern coast of Egypt." *Ain Shams Eng. J.* 9 (4): 3381–3390. https://doi.org/10.1016/j.asej.2018.03.008.

Bloodgood, P. 2017. "Reef building to begin on Piankatank river." *U.S. Army Corps of Eng. Norfolk District*. Accessed June 1, 2019. https://www.nao.usace.army.mil/Media/News-Stories/Article/1175776/reef-building-to-begin-on-piankatank-river/.

Bloodgood, P. 2019. "Chesapeake Bay oyster recovery program." *U.S. Army Corps of Eng. Norfolk District*. Accessed March 10, 2020. https://www.nao.usace.army.mil/About/Projects/Oyster-Restoration.

Blue C Designs. 2015. *BlueDrop operations manual (v1.100)*. Doc. No. 20151119. Halifax, Nova Scotia, Canada: Blue C Designs, Inc.

Brandes, H. G. 2011. "Simple shear behavior of calcareous and quartz sands." *Geotech. Geol. Eng.* 29: 113–126. https://doi.org/10.1007/s10706-010-9357-x.

Briaud, J.-L. 2013. *Geotechnical engineering: Unsaturated and saturated soils*. Hokoben, NJ: Wiley.

Briaud, J.-L., F. C. K. Ting, H. C. Chen, R. Gudavalli, S. Perugu, and G. Wei. 1999. "SRICOS: Prediction of scour rate in cohesive soils at bridge piers." *J. Geotech. Geoenviron. Eng.* 125 (4): 237–246. https://doi.org/10.1061/(ASCE)1090-0241(1999)125:4(237).

Brodie, C. R., M. J. Leng, J. S. L. Casford, C. P. Kendrick, J. M. Lloyd, Z. Yongqiang, and M. I. Bird. 2011. "Evidence for bias in C and N concentrations and $\delta^{13}C$ composition of terrestrial and aquatic organic materials due to pre-analysis acid preparation methods." *Chem. Geol.* 282 (3-4): 67–83. https://doi.org/10.1016/j.chemgeo.2011.01.007.

Bullard, J. E., G. H. McTainsh, and C. Pudmenzky. 2004. "Aeolian abrasion and modes of fine particle production from natural red dune sands: An experimental study." *Sedimentology* 51 (5): 1103–1125. https://doi.org/10.1111/j.1365-3091.2004.00662.x.

Charles, J. A., and M. M. Soares. 1984. "Stability of compacted rockfill slopes." *Géotechnique* 34 (1): 61–70. https://doi.org/10.1680/geot.1984.34.1.61.

Charles, J. A., and K. S. Watts. 1980. "The influence of confining pressure on the shear strength of compacted rockfill." *Géotechnique* 30 (4): 353–367. https://doi.org/10.1680/geot.1980.30.4.353.

Chiew, Y.-M. 1992. "Scour protection at bridge piers." *J. Hydraul. Eng.* 118 (9): 1260–1269. https://doi.org/10.1061/(ASCE)0733-9429(1992)118:9(1260).

Cho, G.-C., J. Dodds, and J. C. Santamarina. 2006. "Particle shape effects on packing density, stiffness, and strength: Natural and crushed sands." *J. Geotech. Geoenviron. Eng.* 132 (5): 591–602. https://doi.org/10.1061/(ASCE)1090-0241(2006)132:5(591).

Coen, L. D., R. D. Brumbaugh, D. Bushek, R. Grizzle, M. W. Luckenbach, M. H. Posey, S. P. Powers, and S. G. Tolley. 2007. "Ecosystem services related to oyster restoration." *Mar. Ecol. Prog. Ser.* 341: 303–307. https://doi.org/10.3354/meps341303.

Consolvo, S., N. Stark, C. F. Castro-Bolinaga, G. Massey, S. Hall, M. Campbell, and M. Thomas. 2020a. "Subaqueous sediment characterization near oyster colonies by means of side-scan sonar imaging and portable free-fall penetrometer." In *Geo-Congress 2020: Geotechnical Earthquake Engineering and Special Topics*, Geotechnical Special Publication 318, edited by J. P. Hambleton, R. Makhnenko, and A. S. Budge, 711–721. Reston, VA: ASCE.

Consolvo, S., N. Stark, C. Castro-Bolinaga, S. Hall, G. Massey, and B. Hatcher. 2020b. *Geotechnical investigation and characterization of bivalve-sediment interactions*. Piankatank River, VA: University Libraries, Virginia Tech.

Crundwell, F. K. 2017. "On the mechanism of the dissolution of quartz and silica in aqueous solutions." *ACS Omega* 2: 1116–1127. https://doi.org/10.1021/acsomega.7b00019.

Cubrinovski, M., and K. Ishihara. 2002. "Maximum and minimum void ratio characteristics of sands." *Soils Found.* 42 (6): 65–78. https://doi.org/10.3208/sandf.42.6_65.

Delgado, S. 2019. "Retrospective analysis of the embayment in the Rachel Carson estuarine research reserve from 1998 to current." M.S. thesis, Nicholas School of the Environment and Earth Sciences, Duke Univ.

De Mello, V. F. B. 1977. "Reflections on design decisions of practical significance to embankment dams." *Géotechnique* 27 (3): 281–355. https://doi.org/10.1680/geot.1977.27.3.281.

Duncan, J. M., S. G. Wright, and T. L. Brandon. 2014. *Soil strength and slope stability*. Hoboken, NJ: Wiley.

Durgunoglu, H. T., and J. K. Mitchell. 1973. *Static penetration resistance of soils*. Research Rep. No. NASA-CR-133460. Washington, DC: NASA Headquarters.

Feinstein, A. R. 1975. "XXXIV. The other side of 'statistical significance': Alpha, beta. delta, and the calculation of sample size." *Clin. Pharmacol. Ther.* 18 (4): 491–505. https://doi.org/10.1002/cpt1975184491.

Fortier, S., and F. C. Scobey. 1926. "Permissible canal velocity." *Trans.* 1588 (89): 940–984.

Galtsoff, P. S. 1964. *The* American oyster Crassostrea V*irginica* G*melin*. Washington, DC: U.S. Government Printing Office.

Goodman, S. 2008. "A dirty dozen: Twelve *P*-value misconceptions." *Semin. Hematol.* 45 (3): 135–140. https://doi.org/10.1053/j.seminhematol.2008.04.003.

Hall, S. A., N. Lenoir, G. Viggiani, J. Desrue, and P. Besuélle. 2009. "Strain localisation in sand under triaxial loading: Characterisation by X-ray micro tomography and 3d digital image correlation." In *Proc., 1st Int. Symp. on Comput. Geomechanics*. New York: ACM, Inc.

Han, J. 2015. *Principles and practices of ground improvement*. Hoboken, NJ: Wiley.

Harding, J. M., R. Mann, M. J. Southworth, and J. A. Wesson. 2010. "Management of the Piankatank river, Virginia, in support of oyster (*Crassostrea Virginica*, Gmelin 1791) fishery repletion." *J. Shellfish Res.* 29 (4): 867–888. https://doi.org/10.2983/035.029.0421.

Haven, D. S., J. P. Whitcomb, and P. C. Kendall. 1981. *The present and potential productivity of the* B*aylor grounds in* V*irginia volume I:* R*appahannock, C*o*rrotoman, G*r*eat* W*icomico,* P*iankatank,* Y*ork and* P*oquoson* R*ivers, and* Mobjack Bay and its tributaries. Special Reports in Applied Marine Science and Ocean Eng. (SRAMSOE) No. 243 v.1. Gloucester Point, VA: Virginia Inst. of Marine Science, College of William and Mary.

Holtz, R. D., W. D. Kovacs, and T. C. Sheahan. 2011. *An introduction to geotechnical engineering*. Upper Saddle River, NJ: Pearson Education Limited.

Holtz, W. G., and H. J. Gibbs. 1956. "Triaxial shear tests on pervious gravelly soils." *J. Soil Mech. Found. Div.* 82 (1): 1–22.

Hunt, H. L., and R. E. Scheibling. 2001. "Predicting wave dislodgment of mussels: Variation in attachment strength with body size, habitat, and

season." *Mar. Ecol. Prog. Ser.* 213: 157–164. https://doi.org/10.3354/meps213157.
Johnson, P. A., and B. M. Ayyub. 1996. "Modeling uncertainty in prediction of pier scour." *J. Hydraul. Eng.* 122 (2): 66–72. https://doi.org/10.1061/(ASCE)0733-9429(1996)122:2(66).
Kirchner, J. W., W. E. Dietrich, F. Iseya, and H. Ikeda. 1990. "The variability of critical shear stress, friction angle, and grain protrusion in water-worked sediments." *Sedimentology* 37 (4): 647–672. https://doi.org/10.1111/j.1365-3091.1990.tb00627.x.
Komada, T., M. R. Anderson, and C. L. Dorfmeier. 2008. "Carbonate removal from coastal sediments for the determination of organic carbon and its isotopic signatures, $\delta^{13}C$ and $\Delta^{14}C$: Comparison of fumigation and direct acidification by hydrochloric acid." *Limnol. Oceanogr. Methods* 6 (6): 254–262. https://doi.org/10.4319/lom.2008.6.254.
Kumar, V., K. G. R. Raju, and N. Vittal. 1999. "Reduction of local scour around bridge piers using slots and collars." *J. Hydraul. Eng.* 125 (12): 1302–1305. https://doi.org/10.1061/(ASCE)0733-9429(1999)125:12(1302).
Kuo, W.-T., H.-Y. Wang, C.-Y. Shu, and D.-S. Su. 2013. "Engineering properties of controlled low-strength materials containing waste oyster shells." *Constr. Build. Mater.* 46: 128–133. https://doi.org/10.1016/j.conbuildmat.2013.04.020.
Kwag, J. M., H. Ochiai, and N. Yasufuku. 1999. "Yielding stress characteristics of carbonate sand in relation to individual particle fragmentation strength." *Eng. Calcareous Sediments* 1: 79–86.
Lade, P. V. 2010. "The mechanics of surficial failure in soil slopes." *Eng. Geol.* 114 (1–2): 57–64. https://doi.org/10.1016/j.enggeo.2010.04.003.
Lambe, T. W., and R. V. Whitman. 1969. *Soil mechanics*. New York: Wiley.
Lee, K. L., and H. B. Seed. 1967. "Drained strength characteristics of sands." *J. Soil Mech. Found. Div.* 93: 117–141. https://doi.org/10.1061/JSFEAQ.0001048.
Li, Y., R. Huang, L. S. Chan, and J. Chen. 2013. "Effects of particle shape on shear strength of clay–gravel mixture." *KSCE J. Civ. Eng.* 17 (4): 712–717. https://doi.org/10.1007/s12205-013-0003-z.
Lipcius, R. N., J. Shen, D. M. Schulte, J. M. Hoenig, and A. M. Colden. 2010. *Ecosystem-based planning of native oyster restoration*. Norfolk, VA: Virginia Institution of Marine Science, College of William and Mary, Final Report to U.S. Army Corps of Engineering.
Margolis, S. V., and D. H. Krinsley. 1971. "Submicroscopic frosting on eolian and subaqueous quartz sand grains." *Geol. Soc. Am. Bull.* 82 (12): 3395–3406. https://doi.org/10.1130/0016-7606(1971)82[3395:SFOEAS]2.0.CO;2.
Massey, G., and C. T. Friedrichs. 2017. *Resistivity,* magnetic susceptibility and sediment characterization of the York river estuary in support of the empirical investigation of the factors influencing marine applications of *EMI (year 2 of SERDP* P*roject MR-2409)* final report. Norfolk, VA: Virginia Instution of Marine Science, College of William and Mary.
McDowell, G. R., and M. D. Bolton. 2000. "Effect of particle size distribution on pile tip resistance in calcareous sand in the geotechnical centrifuge." *Granular Matter* 2 (4): 179–187. https://doi.org/10.1007/PL00010913.
Meyer, D. L., E. C. Townsend, and G. W. Thayer. 1997. "Stabilization and erosion control value of oyster cultch for intertidal marsh." *Restor. Ecol.* 5 (1): 93–99. https://doi.org/10.1046/j.1526-100X.1997.09710.x.
Mulabdic, M. 1993. "Area correction in triaxial testing." *Swedish Geotechnical Inst., Varia 408*. Accessed April 22, 2020. http://www.diva-portal.org/smash/get/diva2:1300328/FULLTEXT01.pdf.
Nandasena, N. A. K., R. Paris, and N. Tanaka. 2011. "Reassessment of hydrodynamic equations: Minimum flow velocity to initiate boulder transport by high energy events (storms, tsunamis)." *Mar. Geol.* 281 (1–4): 70–84. https://doi.org/10.1016/j.margeo.2011.02.005.
NC DEQ (North Carolina Department of Environmental Quality). 2020. Accessed March 11, 2020. https://deq.nc.gov/about/divisions/coastal-management/nc-coastal-reserve/reserve-sites/rachel-carson-reserve.
NOAA (National Oceanic and Atmosphere Administrative). 2018. "Co-OPS Map—NOAA TIDES & currents." Accessed March 18, 2020. https://tidesandcurrents.noaa.gov/map/index.html.
NOAA (National Oceanic and Atmosphere Administrative). 2019. "Water levels—NOAA Tides & Currents" Accessed March 30, 2020. https://tidesandcurrents.noaa.gov/map/index.html?region=Virginia.
Pagán-Ortiz, J. E. 2002. "Impact of the federal highway administration's scour evaluation program in the United States of North America's highway bridges." In *Proc., 1st Int. Conf. Scour Found*, 636–641. College Station, TX. Federal Waterways Engineering and Research Institute.
Perry, J. 1994. "A technique for defining non-linear shear strength envelopes, and their incorporation in a slope stability method of analysis." *Q. J. Eng. Geol. Hydrogeol.* 27 (3): 231–241. https://doi.org/10.1144/GSL.QJEGH.1994.027.P3.04.
Quiah, J., C. Castro-Bolinaga, S. Hall, and N. Stark. 2020. "The impact of excess sediment on bivalve aquaculture." Accessed January 22, 2021. https://content.ces.ncsu.edu/the-impact-of-excess-sediment-on-bivalve-aquaculture.
Reid, D., and M. Church. 2015. "Geomorphic and ecological consequences of riprap placement in river systems." *JAWRA J. Am. Water Resour. Assoc.* 51 (4): 1043–1059. https://doi.org/10.1111/jawr.12279.
Rowe, P. W. 1962. "The stress–dilatancy relation for static equilibrium of an assembly of particles in contact." *Proc. Roy. Soc. A—Math. Phy.* 269 (1339): 500–527.
Schertmann, J. H. 1978. *Guidelines for cone penetration test performance and design*. Rep. No. FHWA-TS-78-209. Washington, DC: U.S. DOT.
Shahnazari, H., and R. Rezvani. 2013. "Effective parameters for the particle breakage of calcareous sands: An experimental study." *Eng. Geol.* 159: 98–105. https://doi.org/10.1016/j.enggeo.2013.03.005.
Stark, N., A. E. Hay, R. Cheel, and C. B. Lake. 2014. "The impact of particle shape on the angle of internal friction and the implications for sediment dynamics at a steep, mixed sand–gravel beach." *Earth Surf. Dyn.* 2 (2): 469–480. https://doi.org/10.5194/esurf-2-469-2014.
Stark, N., A. Kopf, H. Hanff, S. Stegmann, and R. Wilkens. 2009. "Geotechnical investigations of sandy seafloors using dynamic penetrometers." In *Oceans 2009*, 1–10. Biloxi, MS: IEEE.
Stark, N., J. McNinch, H. Wadman, H. C. Graber, A. Albatal, and P. A. Mallas. 2017. "Friction angles at sandy beaches from remote imagery." *Géotechnique Lett.* 7 (4): 292–297. https://doi.org/10.1680/jgele.17.00053.
Stark, N., and T. F. Wever. 2009. "Unraveling subtle details of expendable bottom penetrometer (XBP) deceleration profiles." *Geo-Mar. Lett.* 29 (1): 39–45. https://doi.org/10.1007/s00367-008-0119-1.
Stark, N., R. Wilkens, V. B. Ernstsen, M. Lambers-Huesmann, S. Stegmann, and A. Kopf. 2012. "Geotechnical properties of sandy seafloors and the consequences for dynamic penetrometer interpretations: Quartz sand versus carbonate sand." *Geotech. Geol. Eng.* 30 (1): 1–14. https://doi.org/10.1007/s10706-011-9444-7.
Stephan, S., N. Kaul, and H. Villinger. 2015. "Validation of impact penetrometer data by cone penetration testing and shallow seismic data within the regional geology of the Southern North Sea." *Geo-Mar. Lett.* 35 (3): 203–219. https://doi.org/10.1007/s00367-015-0401-y.
Stoll, R. D., Y.-F. Sun, and I. Bitte. 2007. "Seafloor properties from penetrometer tests." *IEEE J. Oceanic Eng.* 32 (1): 57–63. https://doi.org/10.1109/JOE.2007.890943.
Wardinski, K. M., L. Guertault, G. A. Fox, and C. F. Castro-Bolinaga. 2018. "Suitability of a linear model for predicting cohesive soil detachment during jet erosion tests." *J. Hydrol. Eng.* 23 (9): 06018004. https://doi.org/10.1061/(ASCE)HE.1943-5584.0001690.
Yagiz, S. 2001. "Brief note on the influence of shape and percentage of gravel on the shear strength of sand and gravel mixtures." *Bull. Eng. Geol. Environ.* 60 (4): 321–323. https://doi.org/10.1007/s100640100122.
Yoon, G. L., Y. W. Yoon, and K. S. Chae. 2010. "Shear strength and compressibility of oyster shell–sand mixtures." *Environ. Earth Sci.* 60 (8): 1701–1709. https://doi.org/10.1007/s12665-009-0304-1.
Youd, T. L. 1973. "Factors controlling maximum and minimum densities of sands." In *Evaluation of relative density and its role in geotechnical projects involving cohesionless soils*, edited by E. Selig and R. Ladd, 98–112. West Conshohocken, PA: ASTM.